

A Mathematical Model and Calibration Procedure for Galvanometric Laser Scanning Systems

Alkhazur Manakov¹ Hans-Peter Seidel² Ivo Ihrke^{1,2}

¹Universität des Saarlandes ²MPI Informatik
amanakov@mmci.uni-saarland.de

Abstract

Laser galvanometric scanning systems are commonly used in various fields such as three dimensional scanning, medical imaging, material processing, measurement devices and laser display systems. The systems of such kind suffer from distortions. On top of that they do not have a center of projection, which makes it impossible to use common projector calibration procedures. The paper presents a novel mathematical model to predict the image distortions caused by galvanometric mirror scanning systems. In addition, we describe a calibration procedure for recovering its intrinsic and extrinsic parameters.

1. Introduction

Laser galvanometric scanning systems are used in many different applications. The most widely used application of such kind of system is the barcode reader [BKG*96]. Other applications are laser projection systems [CPP06, KKR03, Wa76], imaging applications [PDJ98, YBP*04, Sta76, Gel03], including medical imaging, material processing [SRGS01, JLR191, CLTL83] and measurement devices [Ger75, WW03]. A laser galvanometric scanning system consists of two mirrors driven by limited-rotation motors. Two mirrors are needed in a two-dimensional scanning system, as shown in Fig. 1. The laser beam enters the system and hits the mirror on the X scanner (first mirror). After reflection, the ray hits the second, Y mirror. By rotating the X mirror, one can control the reflection angle and thus the horizontal coordinate of the outgoing ray. The coordinate along the vertical axis is controlled by the Y scanner. Thus, coordinates of the outgoing ray beam are determined by the rotation angles of the mirrors. In some applications, e.g. in active light 3D-scanning, the positions of the illumination and the camera device are required for triangulation. The calibration of a camera is a well known procedure [Bou05]. If the illumination device is a standard projector, the same calibration procedure can be used as long as the projector has a center of projection. However, a laser galvanometric scanning system does not have a single center of projection and the common calibration procedure can not be used. Applications such as material processing require compensation for distortions in

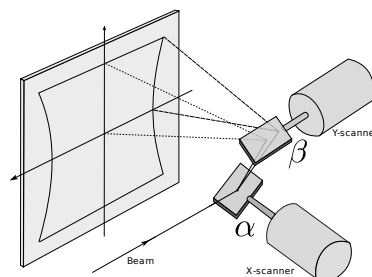


Figure 1: A galvanometric scanning system consists of two mirrors driven by limited-rotation motors. Even in the ideal case, when the incoming ray hits the rotation axes of the mirrors, the system causes distortions.

the whole field of view. Until now this problem was solved by avoiding galvanometric systems where possible e.g. by using two mechanical linear stages for laser ray positioning [Hak90] or by using narrow opening angles [HG07] for which the distortion is negligible.

Unfortunately, the use of linear stages is often impossible and some applications require a large field of view. In other cases compensating for the distortions is performed using polynomial fitting techniques [HFI*08, CCH09]. The polynomial fitting techniques are applicable only if the distance from the system to the object is fixed and the object is planar. This makes polynomial fitting methods not applicable when the calibration needs to be valid for different depths.

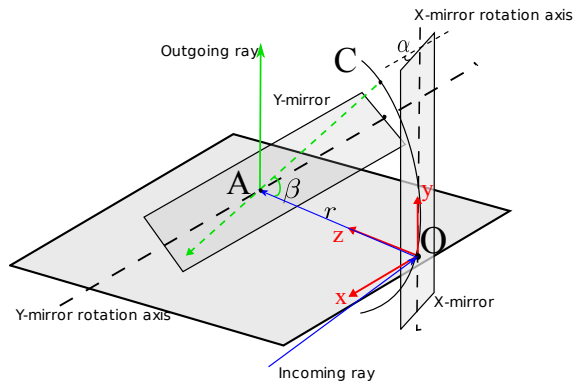


Figure 2: Simple model

In this paper we present a mathematical model to describe laser galvanometric scanning systems. The model describes the distortions introduced by properties of the system and predicts how the distortions will change depending on the parameters of the system. We only consider geometric distortions. Distortions caused by the nonlinear dependence of the mirror rotation angle from a voltage applied to a motor can be calibrated using known procedures [DPN09]. Based on our model, we describe a calibration procedure for estimating the position of the system (rotation and translation matrices) and its internal parameters determining its distortions.

2. Galvanometric scanning system theory

In optics, galvanometric laser control systems are well known and widely used. The distortions they introduce have been described, but mostly for simplified cases [CCH09]. In this paper we present a mathematical model to describe such systems. We start the derivation with a simplified model, exposing the main features of a double mirror scanning system. Though the model can not describe all possible distortions of a galvanometric system it still can be used for calibration, but the result is less accurate. We then extend the model to capture more system distortions and improve the calibration accuracy.

2.1. Simple model

We refer to the mirror that an incoming laser ray hits first as *first mirror* or *X-mirror*: This mirror is usually used for scanning along the horizontal axis. Accordingly, the *second mirror* or *Y-mirror* is the mirror in the system which is used to scan along the vertical axis. To derive a simplified model, we make the following assumptions:

1. The rotation axes of the mirrors are perpendicular,
2. The incoming ray hits the first mirror in the rotation axis,
3. The ray reflected from the first mirror hits the second mirror in the rotation axis, and,

4. The ray is thin in comparison to the mirror dimensions.

The assumptions are still reasonable for real systems because the position of nearly any system can be adjusted so that the incoming ray hits the first mirror in the rotation axis. If the system is designed and assembled well enough, then after reflection by the first mirror, the ray should hit the second mirror in the rotation axis. The assumption concerning the relative dimensions of the mirrors and the beam dimensions is reasonable because the mirrors can be produced large enough to fit the ray. Note, that larger mirror dimensions decrease the scanning speed of the system though. This issue is caused by the inertia of the mirrors: larger mirrors have a larger weight and consequently a larger inertia. A thorough discussion can be found in [TWBv95]. The position of the X-mirror is defined by an angle α . Equally, the position of Y-mirror is described by an angle β . The origin of the laser coordinate system O is located on the rotation axis in the middle of the X-mirror (see Fig. 2). The rotation axis of the Y-mirror is parallel to the X-axis of the coordinate system. The Y-axis coincides with the rotation axis of the X-mirror. The distance between the axes of the mirrors is denoted by r .

Suppose an incoming ray hits the X-mirror in O , intersecting the rotation axis according to the assumptions. Then the coordinates of this point are $O(0;0;0)$. If we rotate the X-mirror, the reflected ray scans a segment along the rotation axis of the Y-mirror. Additionally, O is a projection center for this segment since it does not move while the X-mirror is rotating. Thus, every possible ray in the system passes through O and a point A on the segment parallel to the X-axis. Then the coordinates of A depending on α are $A = (r \cdot \tan \alpha; 0; r)$.

Consider the ray coincident with the Z-axis of the coordinate system before intersection with the Y-mirror. A rotation of the Y-mirror changes the direction of the ray so, that if we imagine a moving laser source O instead of the rotating mirror, it appears to move along an arc with radius r . Let us denote the point moving along the arc as C . The position of C depends on the rotation angle β . The coordinates of C are $(0; r \cdot \sin \beta; r - r \cdot \cos \beta)$. Imagine an outgoing ray from the system. It reflects from the Y-mirror at the point A , but it is simpler to imagine the ray passing through the mirror. This assumption does not change the degrees of freedom of the outgoing ray, but simplifies the equations. Pay attention to the fact that in this case the range of change for β is twice larger. The outgoing ray then passes through A and C , and the ray equation is given by

$$\vec{CA} = \begin{pmatrix} 0 \\ r \cdot \sin \beta \\ r - r \cdot \cos \beta \end{pmatrix} + t \cdot \begin{pmatrix} r \cdot \tan \alpha \\ -r \cdot \sin \beta \\ r \cdot \cos \beta \end{pmatrix}. \quad (1)$$

Imagine we have a screen parallel to the XOY plane at a distance z_0 from the origin. The equation of the plane is $z - z_0 = 0$. Then the intersection point \vec{P} of the ray and the plane

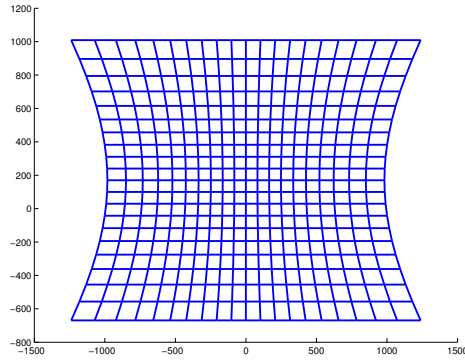


Figure 3: The distortion described by the simple model. Horizontal lines are straight, the grid has vertical and horizontal symmetry.

is

$$\vec{P} = \begin{pmatrix} 0 \\ r \cdot \sin \beta \\ r - r \cdot \cos \beta \end{pmatrix} + \left(\frac{z_0 - r}{r \cdot \cos \beta} + 1 \right) \cdot \begin{pmatrix} r \cdot \tan \alpha \\ -r \cdot \sin \beta \\ r \cdot \cos \beta \end{pmatrix}. \quad (2)$$

Rewriting Eq.(2) explicitly we obtain:

$$\begin{aligned} x &= -r \cdot \tan \alpha \cdot \left(\frac{z_0 - r}{r \cdot \cos \beta} + 1 \right), \\ y &= \frac{(z_0 - r)}{\cos \beta} + r \cdot (1 + \sin \beta), \\ z &= z_0, \end{aligned} \quad (3)$$

with $(x; y; z)$ being the coordinates of \vec{P} in the laser system. The model of Eq.(3) describes distortions as shown in Fig. 3. Note that these distortions appear even in the ideal case where the ray hits the mirrors in the rotation axes. This mathematical model does not describe the situation when an incoming ray hits one or both mirrors out of the rotation axis or when the rotation axes of the mirrors are not perpendicular. These situations are taken into account by the more profound model we propose next.

2.2. Complex model

In the complex model we remove most of the assumptions that we made for the simple model, except that the ray still has to be thin enough to fit onto the mirrors. For the complex model the X-axis is considered to be tilted by γ (see Fig. 4), which is common for modern galvanometric systems. The coordinate system origin is located on the rotation axis of the X-mirror (see Fig. 4). The coordinate system is positioned so that the X-axis is parallel to the rotation axis of the Y-mirror and that the Y-axis is perpendicular to it. As in the simple model, the position of the Y-mirror is defined by the rotation angle β . The current position of the X-mirror is defined by two angles: γ , the incline of the rotation axis is fixed, and the rotation angle α which is describing the motion of the mirror. In addition, the incoming ray can have arbitrary incidence. It is defined by its origin $\vec{S}(s_x; s_y; s_z)$ and by a direction $\vec{l} = (l_x; l_y; l_z)$.

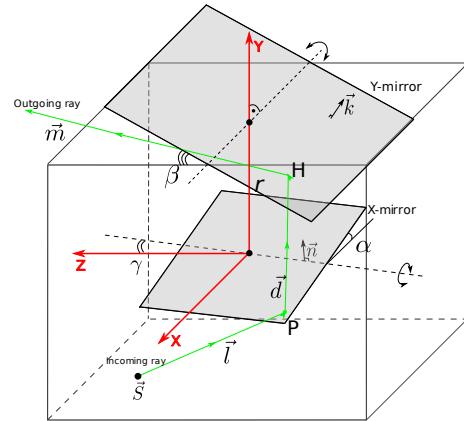


Figure 4: Complex model

To describe the position of the X-mirror, we need the normal and one point on the mirror. The origin of the coordinate system could be taken as a point on the mirror plane $O = (0; 0; 0)$. The normal depends on both γ and α since the rotation is now performed around an inclined axis. Imagine a dashed coordinate system $X'Y'Z'$ which is derived from XYZ by rotating the latter around the X-axis by γ . In the dashed coordinate system, vector $\vec{n}' = (0; 1; 0)$ is a normal for the plane when $\alpha = 0$. In the XYZ coordinate system the same vector is given by $\vec{n} = (0; \cos \gamma; \sin \gamma)$. When changing α , the normal rotates around the Z' -axis. The rotation matrix for this case is

$$R_z = \begin{pmatrix} \cos \alpha & -\sin \alpha & 0 \\ \sin \alpha & \cos \alpha & 0 \\ 0 & 0 & 1 \end{pmatrix}. \quad (4)$$

Thus, the normal in the XYZ system is given by

$$\vec{n} = \begin{pmatrix} -\sin \alpha \\ \cos \alpha \cdot \cos \gamma \\ \cos \alpha \cdot \sin \gamma \end{pmatrix}. \quad (5)$$

The intersection point of the incoming ray with the X-mirror is

$$\vec{P} = \vec{S} + t_x \cdot \vec{l}, \quad t_x = -\frac{(\vec{n}, \vec{O} - \vec{S})}{(\vec{n}, \vec{l})}, \quad (6)$$

where (\cdot, \cdot) denotes the vector scalar product. The ray reflected from the X-mirror has \vec{P} as an origin and the direction \vec{d} of the reflected ray is

$$\vec{d} = 2 \cdot (\vec{n}, -\vec{l}) \cdot \vec{n} + \vec{l}. \quad (7)$$

The normal of the second mirror is

$$\vec{k} = \begin{pmatrix} 0 \\ \cos \beta \\ \sin \beta \end{pmatrix}. \quad (8)$$

As point on the plane it is most convenient to use a point on the rotation axis $\vec{Q} = (0; r; 0)$. Then the intersection of the

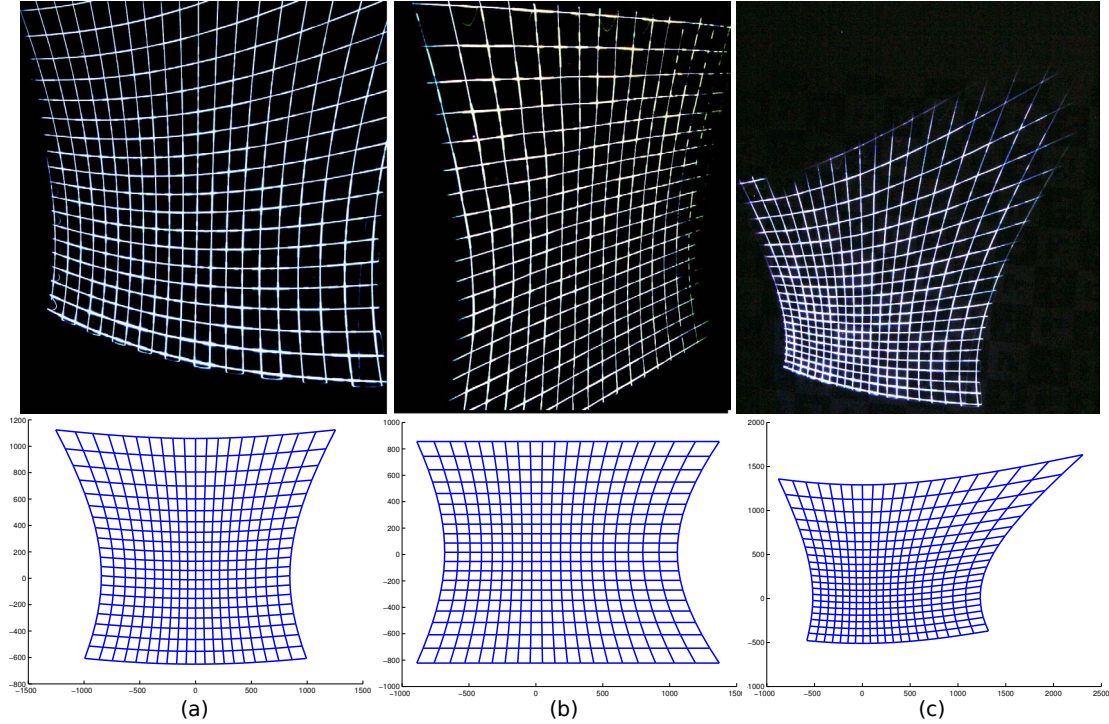


Figure 5: Distortions: top-photographs, bottom-simulations with the complex model. From left to right: (a) Displacement, the ray hits the mirror out of the rotation axis. (b) The ray comes into the system under 15 degrees angle. (c) Combination of the two distortions. Note that the photographs show perspective distortion due to the projection plane being at an angle to the camera's optical axis.

reflected ray with the Y-mirror is given by

$$\vec{H} = \vec{P} + t_y \cdot \vec{d}, \quad t_y = -\frac{(\vec{k}, \vec{Q} - \vec{P})}{(\vec{k}, \vec{d})} \quad (9)$$

The direction of the outgoing ray becomes

$$\vec{m} = 2 \cdot (\vec{k}, \vec{r}) \cdot \vec{k} - \vec{d}. \quad (10)$$

Finally, we obtain the equation of the outgoing ray

$$\vec{R}(t) = \vec{H} + t \cdot \vec{m}. \quad (11)$$

Intersecting the ray with a planar screen parallel to the XOY plane at the distance z_0 from the origin and rewriting the result explicitly we get

$$\begin{aligned} x &= H_x + \frac{z_0 - H_z}{m_z} \cdot m_x, \\ y &= H_y + \frac{z_0 - H_z}{m_z} \cdot m_y, \\ z &= z_0. \end{aligned} \quad (12)$$

This model describes the behavior of a general two-mirror galvanometric system. Note that the complex model reduces to the simple one, Eq.(3), in the following case:

$$\vec{l} = (-1; 0; 0), \quad \vec{S} = (x; 0; 0), \quad \gamma = 0$$

where x can be any positive number.

2.3. Expressiveness of the Complex Model

To show that the complex model is more expressive than the simple one we conduct a number of experiments. We change the parameters of the galvanometric system, rotating and shifting it with respect to the incoming ray. In this case the system causes distortions that the simple model can not express. We project a grid onto a plane and take photographs. Modeling the situation with the complex model, we compare the modeled images and the photographs.

As can be seen from Fig. 5 the complex model is more expressive than the simple one, which supports only the distortions shown in Fig 3. Qualitatively, the real distortions are well captured by our model. Before we show how our model fits real data, Sec. 4, we discuss how its parameters can be estimated from image measurements.

3. Calibration

The parameters describing the system can be divided into two sets: *internal parameters* for properties of the system and *external parameters* to define the position of the system with respect to the camera coordinate system. Consider a galvanometric system more closely for better understanding of the internal parameters. A typical galvanometric system consists of mirrors mounted on galvanometers, motor drivers, a controller and a power supply. The system works

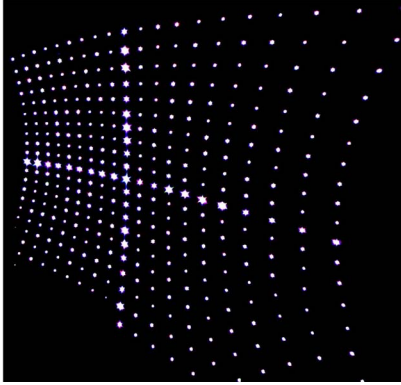


Figure 6: A grid pattern projected onto a planar screen. We project points instead of lines because they are easier and more accurately detectable.

as follows: the controller issues a command for the motor driver to rotate the mirror to a certain angle. The motor driver applies a voltage to rotate the mirror according to the command. Normally, motor drivers are adjusted for a particular motor so that the relation between applied voltage and rotation angle is linear

$$\begin{aligned}\alpha &= s_x \cdot V_x + \alpha_0 \\ \beta &= s_y \cdot V_y + \beta_0\end{aligned}\quad (13)$$

where α is the rotation angle of the X mirror, V_x is the applied voltage, α_0 is an offset of the rotation angle, and s_x is the slope of the line describing the correspondence between V_x and α . The same holds for the other mirror.

In other cases, when the correspondence is not linear it causes additional distortions. In this work we only consider the linear case. However, the linear model can easily be replaced by any other voltage-to-angle mapping model.

One internal parameter of the mirror system is the distance r between the mirrors in the galvanometric system, Fig. 4. Some modern galvanometric systems also have a certain angle γ (different from zero degrees) between the rotation axes of the mirrors, Fig. 4, which also has an influence on the distortions produced by the system. Usually the last two parameters, unlike the slopes and offsets, are given in the manual of the galvo-system. In case they are not mentioned in the manual or have been changed after production, our procedure allows to estimate them. The other two internal parameters which are valid only for the complex model are the origin of the incoming ray \vec{S} and its direction \vec{l} . The external parameters are the rotation and translation matrices of the system with respect to the camera coordinate system.

As raw calibration data we use a point based grid pattern (Fig. 6) projected onto a planar screen, in the following simply called plane. We take N photographs with different plane orientations for the calibration. The points of the pattern are equally spaced in terms of applied voltages. Note that the voltages applied to project the grid must also be recorded

for voltage-to-angle conversion parameter estimation (α, s_x) and (β, s_y). In practice we employ a linear DAC and directly use the DAC values in place of V_x and V_y .

Before we start to estimate the parameters of the projection system we need to compute the three-dimensional coordinates of the projected grid points. We extract the image coordinates of the points and triangulate them. For the triangulation we need to know the position of the plane with respect to the camera. For that purpose it is convenient to have a camera calibration pattern printed on the plane. We denote coordinates of the triangulated points (x_i^j, y_i^j, z_i^j) , where i is the number of the image and j the number of the grid point in an image. $i = 1 \dots N$, $j = 1 \dots M$, where N is the number of photographs and M is the number of laser grid points on the photo. For a simplified exposition we assume that on every photo all the points of the grid are visible and the grid size is $L \times L$ points. The case where not all points are visible is a straight-forward extension. Here and below the coordinates are expressed in camera coordinates if not mentioned otherwise.

3.1. Initial estimation of internal parameters

We start the estimation by computing the parameters of the voltage-to-angle conversion, Eq.(13). To establish this correspondence we need to know the rotation angles, which can be computed from the angles between the outgoing rays. The direction of the rays f^j , $j = 1 \dots M$ can be estimated by fitting a ray to the three-dimensional points of a common index j , measured on different planes. The fitting is performed to the subset of points $W^j = \{w_i^j : i = 1 \dots N\}$, minimizing the error measure

$$E(X^j) = \sum_{i=0}^N (d_j^i)^2, j = 1 \dots M. \quad (14)$$

where d_j^i is the distance from the point W_i^j to the estimated ray. We then measure the angles θ_l^k between the right-most ray f_l^1 and all other rays f_l^k lying on the same horizontal line. Here, $l, k = 1 \dots L$. Similarly, we measure the angles ψ_k^l for the vertical axis the angles between the bottom ray f_1^k and all other rays f_l^k , lying on the same vertical line, where $l = 2 \dots L$ and $k = 1 \dots L$. Having the angles we compute the slopes and the offsets Eq.(15).

$$\begin{aligned}s_x &= \frac{\theta_l^1 - \theta_l^L}{V_x^{\theta_l^1} - V_x^{\theta_l^L}}, & s_y &= \frac{\psi_k^1 - \psi_k^L}{V_y^{\psi_k^1} - V_y^{\psi_k^L}}; \\ \alpha_0 &= \theta_l^1 - s_x \cdot V_x^{\theta_l^1}, & \beta_0 &= \psi_k^1 - s_y \cdot V_y^{\psi_k^1};\end{aligned}\quad (15)$$

$V_x^{\theta_l^k}$ and $V_y^{\psi_k^l}$ are the voltages corresponding to the angles θ_l^k and ψ_k^l .

Estimation of the parameters of the incoming ray is required only for the complex model calibration. The parameters of the incoming ray are estimated by analyzing the shape of the horizontal lines, namely their curvature and stretching

since those strongly depend on the direction of the incoming ray. We generate (compute) a set of rays $h^j, j = 1 \dots M$ using the voltage-to-angle mapping parameters estimated in the previous step using the complex model Eq.(12). Changing only the incoming ray parameters, we minimize the distance between corresponding fitted f^j and generated h^j .

$$E(X^j) = \sum_{i=0}^N (\lambda \cdot (1 - (f^j, h^j)) + d_j)^2, j = 1 \dots M \quad (16)$$

The error to minimize is given by Eq.(16), where d_j is the distance between corresponding rays, computed as a length of a segment perpendicular to both of them. λ is a constant defined as a half of the checkerboard square size. We use the simple model assumptions (Sec. 2.1) as an initial guess for the optimization. To estimate the other internal parameters (for instance, the rotation axis inclination angle and the distance between the mirrors) and to make sure that the estimated internal parameters fit together, we perform a refinement.

We again generate a set of rays $g^j, j = 1 \dots M$ using the internal parameters estimated in the previous step and minimize the error between them and the fitted rays f^j by adjusting the internal parameters of the model. This optimization task can be solved by any suitable optimization method. We use the MATLAB optimization toolbox in our experiments.

In principle, it is possible to perform the internal parameter estimation using only two photographs with full field of view of the projected grid. However, we found that for a stable estimation which converges to reasonable parameters, at least 7 photos are required. It is necessary to include at least one photo with the full field of view for every axis (not necessarily both at once).

3.2. Initial estimation of external parameters

External parameter estimation can be performed with only two photos. Furthermore, it is not necessary to cover the full field of view. The only condition is that the points that lie on the vertical and horizontal central sheets, Fig. 7, must be visible. The *vertical central sheet* is a three-dimensional surface swept in space by the outgoing ray when the X-mirror is fixed in its median position and the Y-mirror scans the whole angular range. Similarly, the *horizontal central sheet* is a three-dimensional surface swept in space by the outgoing ray when the Y-mirror is fixed in its median position and the X-mirror scans the whole angular range. The *YOZ* and *XOZ* planes expressed in laser coordinates are tangent planes, Fig. 7, to the vertical and horizontal central sheets.

The ray which results if both mirrors are in their median positions is the intersection of the tangent planes to the central sheets and is called the *optical axis*. Note that in the simple model case the tangent planes are equal to the central sheets. Thus, the procedure is the same for both models. We consider the solution for the complex model and it can be reduced to the simple one.

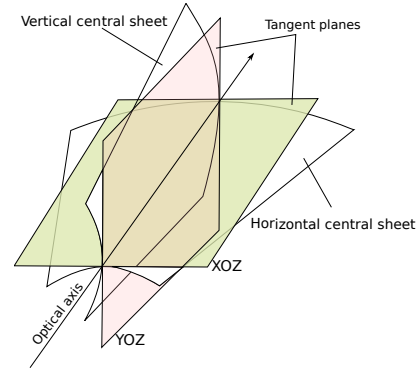


Figure 7: Central sheets and planes

The goal is to estimate the orientation of the laser coordinate system and the position of its origin. The main idea is to estimate the optical axis first and then fit the *YOZ* and *XOZ* tangent planes to the central sheets. The origin can be computed using the model and the 3D-points given in camera coordinates together with the fact that the projection of a point onto the tangent planes are the X- and Y-coordinates expressed in the laser coordinates.

To estimate the optical axis we select the points D_i^{med} , $i = 1 \dots N$ corresponding to the intersection of the planar screen and the ray which results if both mirrors are in their median positions. The optical axis is fitted to the points minimizing the distance given by Eq.(14). For tangent plane estimation, we select the points on the median grid lines (lines corresponding to the median voltage values) B_i^v and B_j^h , $i = 1 \dots L \cdot N, j = 1 \dots L \cdot N$. Then, we fit the tangent planes to the central sheets in such a way that they pass through the optical axis, remain perpendicular to each other and the squared distance between the plane and the corresponding points (B_i^v and B_j^h) is minimal. The error is computed according to Eq.(17), where d_i is the distance from the point to the corresponding tangent plane. As a result we obtain normals \vec{n}_v and \vec{n}_h and a point on every tangent plane.

$$E(X^j) = \sum_{i=0}^{L \cdot N} (d_i)^2. \quad (17)$$

We define the Z-axis of the galvanometric system as the optical axis. Once we have computed the tangent planes, we know the three vectors (the normals to the planes \vec{n}_v and \vec{n}_h and the optical axis). Therefore, we can fix the rotational degrees of freedom of the system. Thus the rotation matrix R is a matrix composed of those vectors in the following way:

$$R = (\vec{n}_v | \vec{n}_h | (\vec{n}_v \times \vec{n}_h)), \quad (18)$$

where $(\cdot \times \cdot)$ denotes the cross product. To estimate the position of the origin of the system, we need to know the coordinates of the points $(x_i^j; y_i^j; z_i^j)$ given in the laser coordinate system. Knowing the orientation of the galvanometric system R , we can compute the projections $(p_i^j; q_i^j)$ of the points $(x_i^j; y_i^j; z_i^j)$ onto both tangent planes. The projections are the

coordinates of the points expressed in the laser coordinate system. The missing Z-coordinate can be computed using the model, the estimated internal parameters, and the measured voltages for every pair $(p_i^j; q_i^j)$. Note that the distance is from the j^{th} point to the origin of the laser coordinate system. We use the median Z-value of the points lying on the optical axis as a guess for the origin of the laser coordinate system.

3.3. Parameter refinement

As mentioned above, the refinement is performed simultaneously for the external and internal parameters. The refinement is another minimization task. The goal is to know how the system converts applied voltages into an equation of the outgoing ray. We have a set of voltages (V_x, V_y) , which we used to project the pattern and the response of the system (photographs with the pattern projected on the plane). Thus we can adjust the parameters of the model of the system so, that the response of the model coincides with the response of the real system as well as possible. The sum of the distances between the points predicted by the model and the experimentally measured ones is used as the error measure. Note that the distance can be computed in camera image space or in three-dimensional space.

4. Experimental validation

To validate the developed model and calibration procedure we performed two experiments. The first is calibration, meaning estimation of all system parameters. In the second experiment we use a calibrated system to perform rectified projection onto a curved surface.

4.1. Calibration experiment

The validation is conducted in a leave-one-out fashion. We take 10 photographs, but use only 7 to perform the calibration. The accuracy is then measured for the remaining 3 photographs.

For the validation of the calibration procedure we chose a combined distortion case. The incoming laser ray is displaced from the rotation axes of the mirrors and enters the system under a certain angle with the X-axis, Fig. 4. The distortions for this case are shown in Sec. 2.3, see Fig. 5. In this case, the grid is asymmetric, it has neither vertical nor horizontal symmetry. Despite the fact that the applied voltages are equidistant, the distances between the corners are different. Furthermore, we can not see the whole grid because at a certain angle of rotation the ray leaves the mirror. Following the calibration procedure described in Sec. 3, we take photos of the projected grid, Fig. 6. The brighter points correspond to median values of the applied voltages. We also take photographs with the plane under good illumination to determine its position with respect to the camera. The detection of the calibration pattern is implemented in MATLAB. Assuming that the intensity inside of the beam is distributed

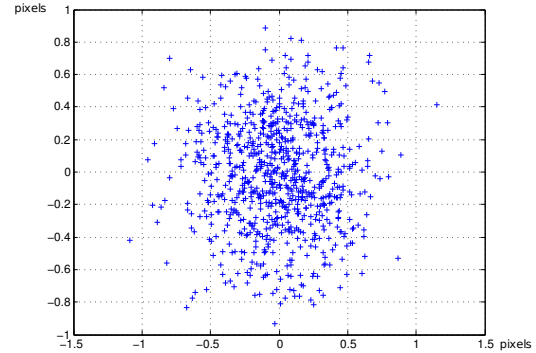


Figure 8: Error distribution

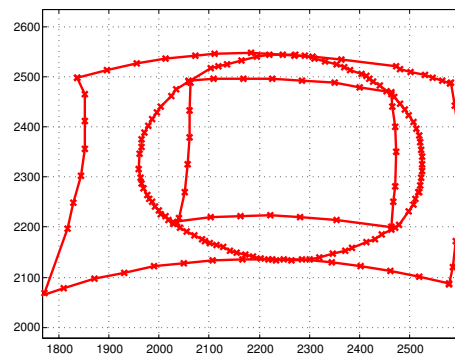


Figure 9: Top: The rectified pattern in laser coordinates. Note: Marked points are provided the remained is interpolated by physical motion the galvo system.

as a Gaussian, we detect the center of the spot. After calibration of the system we predict the points on the planes that we did not use for calibration. The error measure is

$$E = \frac{1}{M} \sum_{i=0}^M (x_i - p_i)^2, \quad (19)$$

where M is the number of points for which the error is computed, x_i are the measured points, and p_i are the model predicted points. The error is computed in image coordinates and expressed in pixels. The number of points we used for validation is 277. The maximum error per point is 1.2 pixels or 30% of the laser beam width. The average error among all points on the plane is 0.96 pixel, or 27% of the laser beam width. A plot of the error distribution is shown in Fig. 8.

4.2. Projection experiment

Using our model and the complete calibration information, including internal parameters, we can rectify any pattern in such a way, that, while projecting onto a curved surface, the pattern appears straight from one particular view-point, (see Fig. 10). For our experiment we used a sphere with a diameter of 23.4 cm. The setup consists of a calibrated camera, a laser-galvanometric system and the sphere (see Fig. 10). The rectified pattern we project, represented in laser coordinates is shown in the Fig. 9.

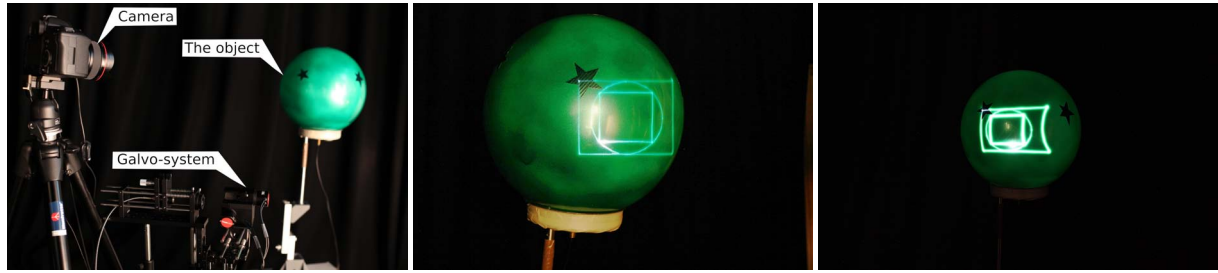


Figure 10: Projection experiment. From left to right: The setup: the camera, the laser and the sphere; view from the camera, the pattern is straight; view from a different camera perspective, the pattern is distorted.

The rectification is done as follows: Suppose we have a pattern given by a set of points $U = \{u_i : i = 1 \dots N\}$ in the camera image coordinate system and a description of the object geometry. We virtually project the desired pattern from the camera view onto the object geometry. The intersection is given by a set of three dimensional points $\{x'_i : i = 1 \dots N\}$. These are then converted to the laser coordinate system $x_i = R^{-1}(x'_i - T)$, where R and T are rotation and translation matrices to convert from the laser coordinate system to the camera coordinate system. By inverting Eq.(12) and computing the required voltages $V = V_x^i, V_y^i, i = 1 \dots N$, we can project a rectified pattern onto the surface. This experiment shows one possible application of our laser model. Note that for this experiment we also used the combined distortion system. The results are shown in Fig. 10.

5. Conclusion

In this work, we present two mathematical models to describe the behavior of galvanometric laser scanners and an associated calibration technique for computing their parameters in real setups. The distinctive feature of the proposed calibration method is that it uses a mathematical model of the galvanometric system. The use of a mathematical model allows the computation of a calibration which is valid for a whole range of depths. Although the simple model is not expressive enough since it is able to describe only one type of distortions that can occur, it can be used for calibration of systems for which the assumptions are valid. The complex model is more expressive and can handle all the distortions introduced by a galvanometric scanning system.

References

- [BKG*96] BRIDGELALL R., KATZ J., GOREN D., DVORKIS P., LI Y.: Laser scanning system and scanning method for reading 1-d and 2-d barcode symbols.
- [Bou05] BOUGUET J.-Y.: Camera Calibration Toolbox for Matlab, 2005.
- [CCH09] CHEN M.-F., CHEN Y.-P., HSIAO W.-T.: Correction of field distortion of laser marking systems using surface compensation function. *Optics and Lasers in Engineering* 47, 1 (2009), 84 – 89.
- [CLTL83] CELLER G. K., LEAMY H. J., TRIMBLE, LEE E.:

Method of increasing the grain size of polycrystalline materials by directed energy-beams, September 1983.

- [CPP06] CALLISON J. P., PEASE J. S., PEASE R. W.: Laser projection system, November 2006.
- [DPN09] DUMA V. F., PODOLEANU A. G., NICOLOV M.: Modeling a galvoscaner with an optimized scanning function. 539–548.
- [Gel03] GELBART D.: Method for imaging a continuously moving object, December 2003.
- [Ger75] GERHARD W.: Method and apparatus for measuring the distance and/or relative elevation between two points in an opto-electronic manner, August 1975.
- [Hak90] HAKKY S. I.: Laser resectoscope with mechanical and laser cutting means, September 1990.
- [HFI*08] HULLIN M. B., FUCHS M., IHRKE I., SEIDEL H.-P., LENSCH H. P. A.: Fluorescent immersion range scanning. *ACM Trans. Graph. (Proc. SIGGRAPH 2008)* 27, 3 (2008), 87:1–87:10.
- [HG07] HELMCHEN F., GO W.: Imaging cellular network dynamics in three dimensions using fast 3d laser scanning. *Nature Methods* 4, 1 (2007), 73–79.
- [JLR191] JOHNSON J. C., LO H., ROWLEY D., IRLAND T.: Method and apparatus for laser processing a target material to provide a uniformly smooth, continuous trim profile, October 1991.
- [KKR03] KURTZ A. F., KRUSCHWITZ B. E., RAMANUJAN S.: Laser projection display system, June 2003.
- [PDJ98] PODOLEANU A. G., DOBRE G. M., JACKSON D. A.: En-face coherence imaging using galvanometer scanner modulation. *Optics Letters* 23 (Feb. 1998), 147–149.
- [SRGS01] SUKMAN Y. P., RISSER C. J., GORHAM E. W., SCHULTZ D. W.: Laser material processing system with multiple laser sources apparatus and method, November 2001.
- [Sta76] STARKWEATHER G. K.: Scanning system for imaging characters combined with graphic curves, August 1976.
- [TWBv95] TUMER I., WOOD K. L., BUSCH-VISHNIAC I. J.: Modeling of dynamic effects caused by the beam delivery system in selective laser sintering. In *Proceedings of the 1995 Solid Freeform Fabrication Symposium* (Aug. 1995), pp. 353–361.
- [Wa76] WHITBY C. M., AND D. L. W.: Combined laser recording and color projection system, June 1976.
- [WW03] WULF O., WAGNER B.: Fast 3d scanning methods for laser measurement systems. 3–8.
- [YBP*04] YUN S., BOUDOUX C., PIERCE M., DE BOER J., TEARNEY G., BOUMA B.: Extended-cavity semiconductor wavelength-swept laser for biomedical imaging. *Photonics Technology Letters, IEEE* 16, 1 (jan. 2004), 293 –295.